A Physics-Informed Gaussian Process Regression-Based Meta Model for Rapid Characterization of Permanent Magnet Synchronous Machines

Marcelo D. Silva*, Oluwaseun A. Badewa†, Rosemary E. Alden†, Pedram Asef‡, Dan M. Ionel†, Sandra Eriksson*

*Department of Electrical Engineering, Uppsala University, Uppsala, Sweden.
marcelo.silva@angstrom.uu.se, sandra.eriksson@uu.se
†SPARK Laboratory, University of Kentucky, Lexington, KY, USA
o.badewa@uky.edu, rosemary.alden@uky.edu, dan.ionel@ieee.org
‡e-Motion Laboratory, Advanced Propulsion Laboratory (APL), University College London, London, UK
pedram.asef@ucl.ac.uk

***Abstract*—Optimizing an Interior Permanent Magnet Synchronous Machine (IPM) requires evaluating multiple working points for each candidate design. In case the design domain has many dimensions, multiple working points evaluations would require an impractical number of finite element method (FEM)-based simulations. This study proposes a novel strategy to build a meta-model to reduce the number of FEM-based simulations for a given optimization process. The study proposes a novel, physics-informed meta-model based on Gaussian Process Regression (GPR) aiming for rapid characterization of any given machine design. The meta-model uses an adapted version of Posterior Standard Deviation (PSD) to allow for an exact and detailed adaptive sampling strategy. The results show that the proposed meta-model presents a data-efficient approach capable of computing performance parameters with low error. Additionally, the characterization from the proposed meta-model agrees with the experimental data.**

***Index Terms*—Gaussian Process Regression, Meta-Model, IPM, Experimental Verification, Physics-Informed Characterization, Design Optimization, Drive Cycle**

I. Introduction

Interior Permanent Magnet Synchronous Machines (IPMs) are widely used in high-performance applications across multiple operating points. Optimizing an IPM involves evaluating each candidate design's performance across all working points. While Finite Element Method (FEM)-based models are the standard for these evaluations, conducting a large number of FEM simulations can be computationally impractical [1] [2] [3], mainly if the design domain has several dimensions.

To address this challenge, meta-models have been developed to approximate FEM simulation results at a much lower computational cost [1] [4] [5]. Previous studies demonstrate the effectiveness of the use of meta-models for IPM optimization [6] and characterization [7] across multiple working points by significantly reducing the number of FEM-based simulations. These previously proposed meta-models can be based on polynomial regression [7], artificial neural networks (ANN) [8], Gaussian Process Regression (GPR) [9], or multiple others.

Yet, studies aiming to characterize IPMs efficiently [7] [10] are not able to generalize for different IPM designs. Instead, these studies show their efficiency for only one design. Similarly, the models focusing on optimization are bounded by an initial working points selection, e.g., a specific drive cycle, [6] [11]. Requiring a different data set to train the meta-model in the case the drive cycle is updated or changed. Thus, this gap in current meta-modeling approaches can be filled by a meta-model that adapts to any selection of working points or drive cycles while accommodating various geometries, i.e., capable of being used efficiently for both fast characterization of a design and optimization given any drive cycle.

This study introduces a novel meta-model strategy to estimate performance parameters for any given IPM design, allowing a fast evaluation of a design for any drive cycle. It achieves this by combining Gaussian Process Regression (GPR) with governing physical equations. Also, it is proposed a variation on the traditional adaptive sampling policy Posterior Standard Deviation (PSD) to take into consideration input-output dependencies and allow for a precise adaptive sampling strategy. GPR has been employed in simpler meta-models [1] or in other IPM-related applications [9]. This study leverages its capabilities to develop a more powerful meta-model.

The following section II introduces the spoke-type IPM (spoke) machine used. Next, the GPR's fundamentals and its implementation details are described in section III. In section IV, the novel meta-model strategy is described, together with the physical governing equations used and the conditions under which the training data was gathered. Finally, section V presents and analyzes the performance of both the GPR framework and the whole meta-model.

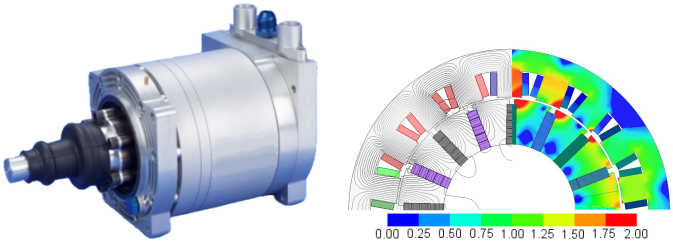

Fig. 1: The ultra-high specific torque IPM motor is considered as the reference for the study. Prototype from the original developments for the first generation Formula E (a) and the magnetic field in the motor cross section, flux lines and flux density in excess of 2T, illustrating the heavy saturation (b).

II. Reference IPM Motors

The current study employs as a reference example a prototype IPM motor, which was designed and prototyped from the original developments for the first generation Formula E and further optimized as described in more detail in [6] and [12]. The IPM motor has a spoke rotor with 16 poles and a 3-phase winding with concentrated coils placed around 18 teeth, as shown in Fig. 1. The motor can operate to a maximum of 110Nm, 12000rpm, and 325Arms with a 650V DC bus [12], and a base speed of 3500 rpm was considered in this study. The design, which set a record high specific torque, has very high magnetic saturation that recommends it for a challenging study involving nonlinearities.

From this prototype, eight geometric variables were included in the design domain. The range of values for these variables is detailed in Table I, where k_{si} is the quotient between the stator inner and outer diameter; h_g, the air gap length; k_{w_t}, the quotient between the stator teeth width and its maximum; $k_{h_{pm}}$, the quotient between the PMs' height and the maximum for PMs' height; $k_{w_{pm}}$, the quotient between the PMs width with the rotor pole; $k_{w_{br}}$, the proportion of the rotor slot opening in relation to the PMs' width; d_{br}, the distance between the rotor's surface and the PMs' top; and h_y, the distance between the top of the stator slot and the outer stator diameter.

III. Gaussian Process Regression

A Gaussian process ($\mathcal{GP}$) employs a set of random variables characterized by a multivariate normal distribution, making it useful for regression tasks by fitting the $\mathcal{GP}$ to the available training data [13]. A $\mathcal{GP}$ can be expressed as:

$$f(\mathbf{x}) \sim \mathcal{GP}(m(\mathbf{x}), k(\mathbf{x}, \mathbf{x}')), \tag{1}$$

where $m(\boldsymbol{x})$ is the mean function; and $k(\mathbf{x}, \mathbf{x}')$, the covariance function. The mean function $m(\mathbf{x})$ is defined as linear:

$$m(\mathbf{x}) = W\mathbf{x} + B, \tag{2}$$

where W and B are constants learned during training.

Given such characteristics of $\mathcal{GP}$, the new observations, $\mathbf{x}' = [i_d, i_q, \omega_e]$, can also be described by a normal distribution. Resulting in:

TABLE I: Details on Geometric Variables

Variables	Maximum	Minimum	Prototype
k_{si} [-]	0.75	0.6	0.704
h_g [mm]	2.5	0.7	1
k_{w_t} [-]	0.75	0.45	0.662
$k_{h_{pm}}$ [-]	0.95	0.55	0.775
$k_{w_{pm}}$ [-]	0.6	0.2	0.388
$k_{w_{br}}$ [-]	0.65	0.35	0.5
d_{br} [mm]	3	1.5	2.5
h_y [mm]	15	7	10.7

$$\lambda_d(x') \sim \mathcal{N}(\mu_d, \sigma_d^2), \tag{3}$$

$$\lambda_q(x') \sim \mathcal{N}(\mu_q, \sigma_q^2), \tag{4}$$

for the flux linkage maps prediction. The loss component predictions can also be described similarly by a normal distribution. Thus, the use of GPR provides a value for the regression task and also the variance $\mathbb{V}$ of a regression task. The $\mathbb{V}$ can be used in adaptive sampling methods, as is the case in this study (detailed in Section IV).

The mean function is computed independently for each of the input dimensions. For the covariance function, $k(\mathbf{x}, \mathbf{x}')$, the $Matérn$ 5/2 *kernel* was implemented since it presented the best performance. For this particular study, since the training data has its origin in FEM-based simulations, it is noise-free, which eliminates inter-task transfer effects [5]; thus, each output is modeled as an independent $\mathcal{GP}$. The data is normalized before it is used to fit the $\mathcal{GP}$s used in this study.

IV. Novel Meta-Modeling Structure and Strategy

The proposed meta-modeling technique based on GPR and governing physical equations consisted of two modules, as illustrated in Fig. 2. The first module is designed to define which working points (i_d, i_q, ω_e, where $i_d = -I_{ph}sin(\gamma)$; $i_q = I_{ph}cos(\gamma)$; ω_e, the electrical speed; γ, the rotor electrical angle in relation to the stator D-axis; and i_{ph}, the module current) are required to efficiently compute the linkage flux maps in Q, $\psi_q(i_d, i_q)$, and D-axis, $\psi_d(i_d, i_q)$, and the several loss components. The loss components are the stator winding copper losses, L_{copper}, core losses, L_{core}, and the eddy losses in the PMs, L_{solid}. These loss components are quantified using the FEM models [6]. This stage is executed for a single design, and the working points defined here are used for the designs to be used in the second module.

The second module is established to relate geometric variables and $\psi_q(i_d, i_q)$, $\psi_d(i_d, i_q)$, and losses. This relation combines the data of different designs at the same working point and fitting independent geometry $\mathcal{GP}$s for the different working points determined in the first module. Running all of these GPRs allows the meta-model to compute the efficiency maps for any given geometry within the design domain.

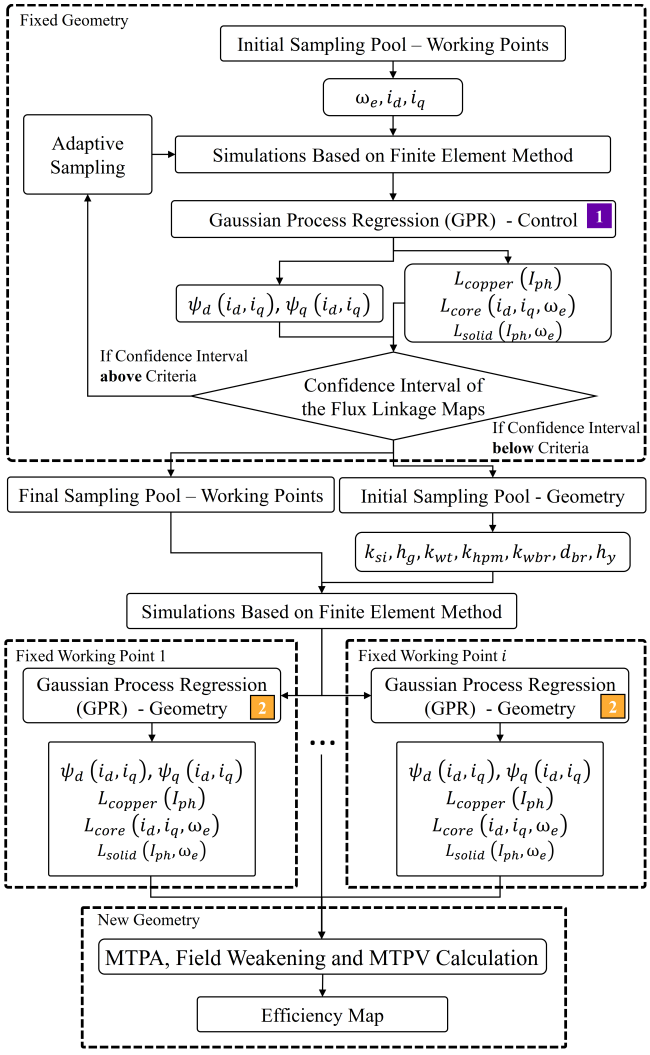

Fig. 2: Illustration of the novel meta-model structure proposed in this study.

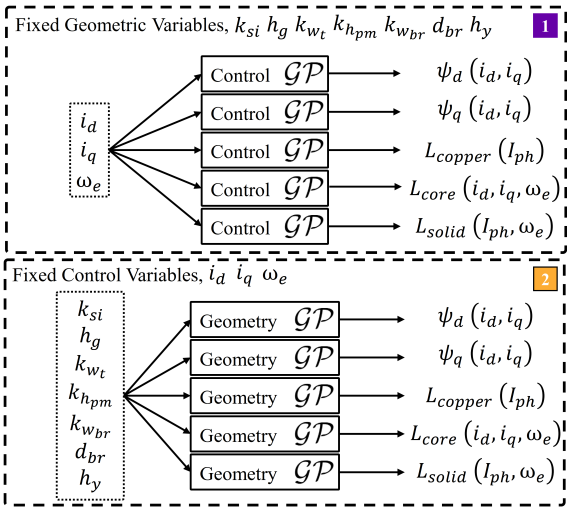

Fig. 3: Illustration of the independent control $\mathcal{GP}$s (a). Illustration of the independent geometry $\mathcal{GP}$s (b). The number on the upper right corner identifies were these $\mathcal{GP}$s fit in Fig 2.

TABLE II: Pearson Correlation Coefficient

	I_d **[A]**	I_q **[A]**	ω_e **[Hz]**
ψ_d [Wb]	1.00	-0.03	0.00
ψ_q [Wb]	-0.02	1.00	0.00
L_{copper} [W]	-0.67	0.67	0.00
L_{solid} [W]	-0.41	0.41	0.55
L_{core} [W]	0.02	0.51	0.73

For the first module, the initial sampling was defined by using Latin Hypercube Sampling (LHS), together with the sampling of the domain limits. The adaptive sampling was based on the GPR's output variance, as defined in Section III. For 1D GPR problems, PSD is a common approach to adaptive sampling. However, given the five independent outputs ($\psi_q(i_d, i_q)$, $\psi_d(i_d, i_q)$, and loss components), a standard application of PSD would result in five new sampling points for the next round, which does not allow for a precise adaptive sampling strategy. Furthermore, not all the outputs are affected by the three inputs (i_d, i_q, ω_e) in the same way.

To quantify the relation between inputs and outputs, Pearson Correlation Coefficients (PCC) were used, and are detailed in Table II. Additionally, for each independent control $\mathcal{GP}$s, the output $\mathbb{V}$ was computed for the whole input domain. Followed by the selection of the input coordinates that result in the highest output $\mathbb{V}$, these coordinates are:

$$\mathbf{x}^j_{\mathbb{V}_{max}} = [i^j_{d(\mathbb{V}_{max})}, i^j_{q(\mathbb{V}_{max})}, \omega^j_{e(\mathbb{V}_{max})}], \tag{5}$$

where j corresponds to the outputs of the independent control $\mathcal{GP}$s. The inputs corresponding to the most uncertainty for each of the independent control $\mathcal{GP}$s (($\psi_q(i_d, i_q)$, $\psi_d(i_d, i_q)$ and loss components)) is now known. Thus, each input coordinate, i, of the new sampling points is computed as follows:

$$x'_i = \sum_j \mathbb{P}_{ij} \mathbb{V}_{max,ij} x^j_{\mathbb{V}_{max},i}, i \in [0, 2], \tag{6}$$

where $\mathbb{P}$ is the PCC matrix; $\mathbb{V}_{max}$, the maximum variance matrix; i, the index identifying the input coordinate; and j, is the index identifying the independent control $\mathcal{GP}$s. For the adaptive sampling process, $\mathbb{P}$ and $\mathbb{V}_{max}$ are normalized.

Regarding the second module, the working points defined in the previous module were simulated for each of the geometries. The geometries included were defined using LHS. In the second module, independent geometry $\mathcal{GP}$s are defined, one per working point and performance outputs ($\psi_q(i_d, i_q)$, $\psi_d(i_d, i_q)$ and loss components). These have the geometry parameters, described in Section II, as inputs and the same outputs defined for independent control $\mathcal{GP}$s. The schematic of both control and geometry $\mathcal{GP}$ is illustrated in Fig. 3

Given that none of the $\mathcal{GP}$ defined in this meta-model computes torque or voltages, governing physical equations are needed to determine the performance of each of the designs

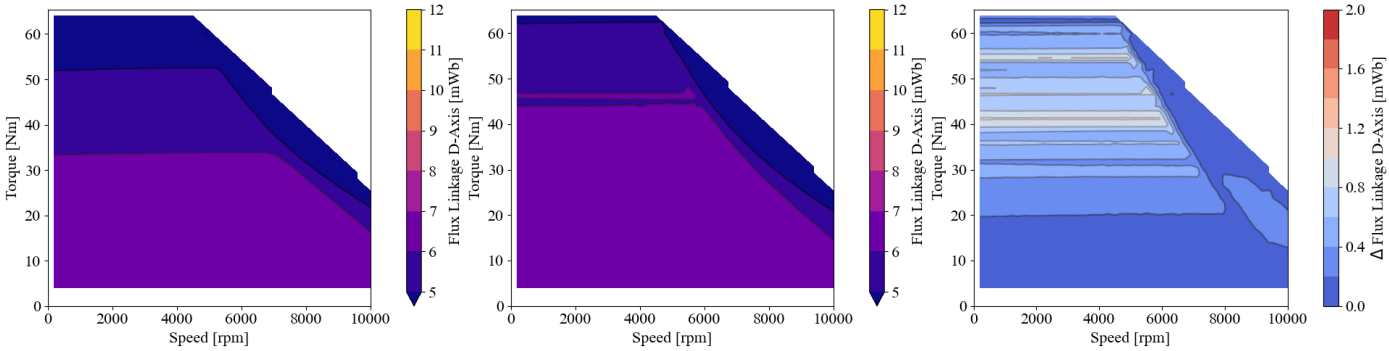

Fig. 4: Left (a): ψ_d map using 256 FEM simulations. Middle (b): ψ_d map from the meta-model's first module output using 6/14 FEM simulations. Right (c): Difference, in mWb, between the two ψ_d maps.

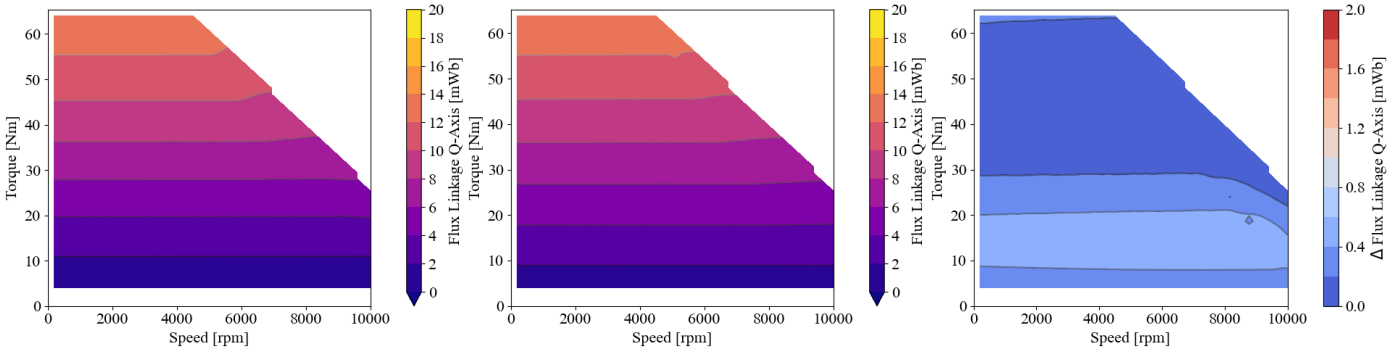

Fig. 5: Left (a): ψ_q map using 256 FEM simulations. Middle (b): ψ_q map from the meta-model's first module output using 6/14 FEM simulations. Right (c): difference, in mWb, between the two ψ_q maps.

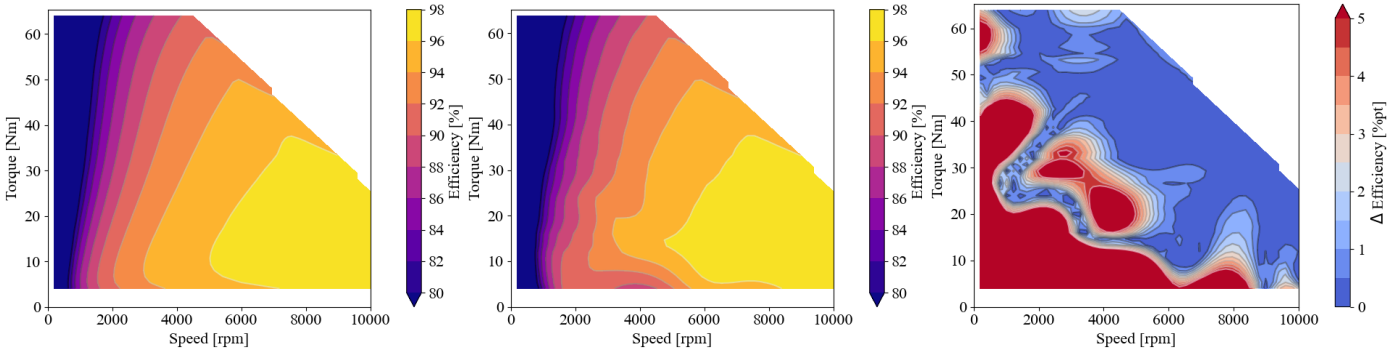

Fig. 6: Left (a): Efficiency map using 256 FEM simulations. Middle (b): Efficiency map from the meta-model's first module output using 6/14 FEM simulations. Right (c): Difference, in %pt, between the two efficiency maps.

evaluated using it. Torque can be defined as:

$$T_e = 1.5p[\psi_d(i_d, i_q)i_q - \psi_q(i_d, i_q)i_d], \tag{7}$$

where T_e is the electromagnetic torque and p is the number of pole pairs. Additionally, the voltage equations are:

$$v_d = R_s i_d + \frac{d\psi_d(i_d, i_q)}{dt} - \omega_e \psi_q(i_d, i_q), \tag{8}$$

$$v_q = R_s i_q + \frac{d\psi_q(i_d, i_q)}{dt} - \omega_e \psi_d(i_d, i_q), \tag{9}$$

where v_d and v_q are the peak fundamental voltage on the d-axis and q-axis, respectively; R_s, the phase resistance; and ω_e, the electrical speed. For each working point in the efficiency maps, i_d and i_q values were determined using Maximum Torque per Ampere, Field Weakening, and Maximum Torque per Voltage strategies. The training and test data were generated from 2D FEM using *Ansys Electronics Desktop 2023*.

V. Results and Discussion

As discussed in the previous Section IV, the proposed meta-model is divided into two modules. In the first module, the goal is to determine which working points are needed to

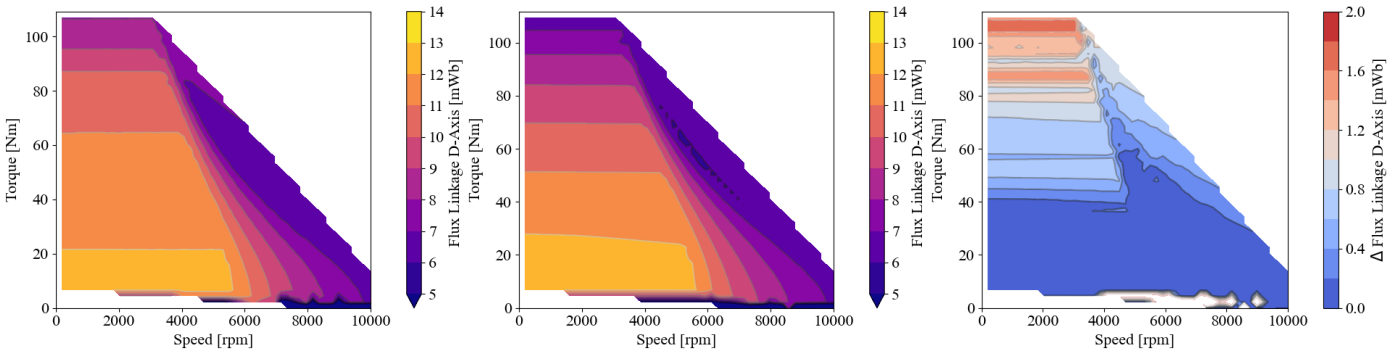

Fig. 7: Left (a): ψ_d map using 256 FEM simulations. Middle (b): ψ_d map from the meta-model's second module output, without any dedicated FEM simulation. Right (c): difference, in mWb, between the two ψ_d maps.

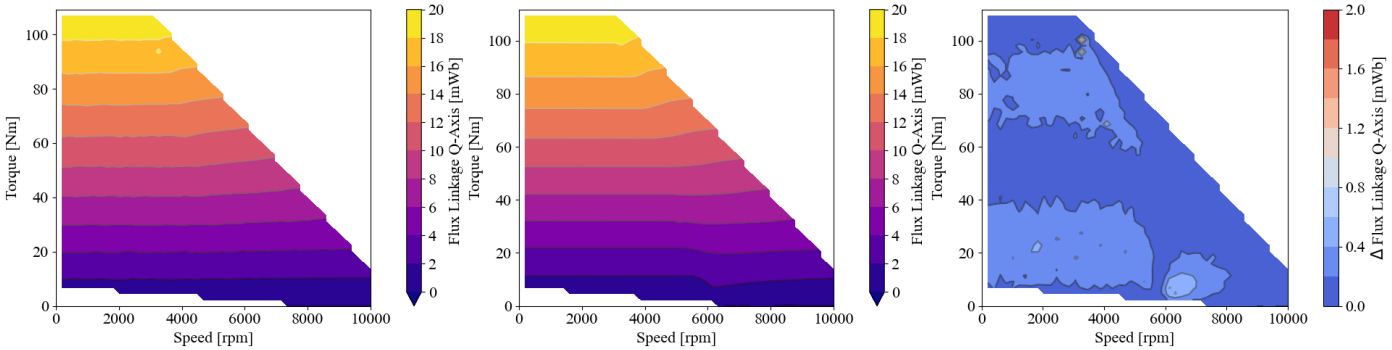

Fig. 8: Left (a): ψ_q map using 256 FEM simulations. Middle (b): ψ_q map from the meta-model's second module output, without any dedicated FEM simulation. Right (c): difference, in mWb, between the two ψ_q maps.

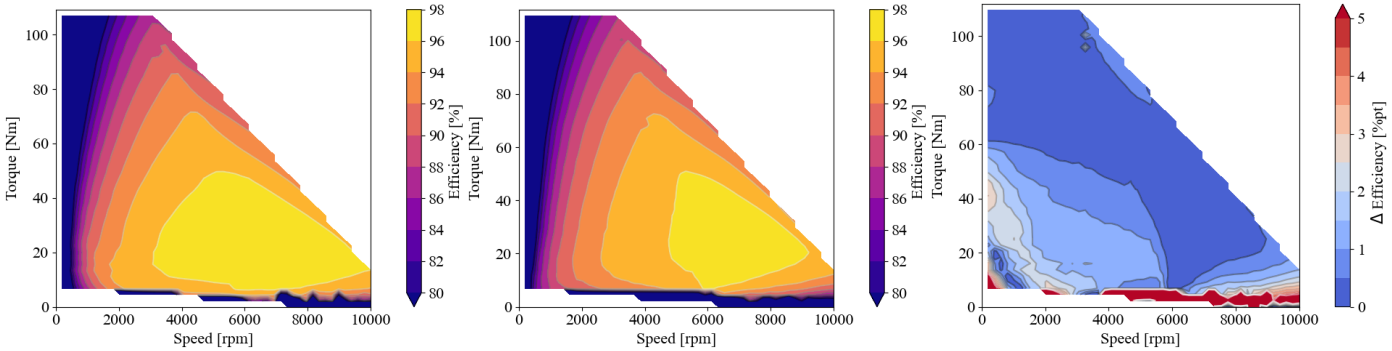

Fig. 9: Left (a): efficiency map using 256 FEM simulations. Middle (b): efficiency map from the meta-model's second module output, without any dedicated FEM simulation. Right (c): difference, in %pt, between the two efficiency maps.

characterize one design; in the second module, the goal is to characterize any new geometry within the design domain.

A. *Meta-Model Performance*

1) GPR Control - Fix Geometry, Multiple Working Points: For the first module, the best-performing combination of some initial sampling and the total budget was 6 and 14 FEM simulations, respectively. Using only the first module of the meta-model, it is possible to calculate the efficiency map of the fixed geometry used during this module. The efficiency map is presented in Fig. 6b. Compared with the efficiency map based on 256 FEM simulations, in Fig 6a. Deviations around 5%pt are observed in low torque and low speed working points, which are of reduced use, Fig. 6c. Thus, the methodology, the adaptive sampling, and the use of 14 FEM simulation is a good choice before proceeding to the second module.

The ψ_d and ψ_q maps for each working point are illustrated in Figs. 4 and 5, respectively. For the flux linkages, the agreement is good across the whole domain, as can be seen in Fig. 4c and Fig. 5c. Thus, the disparity in the efficiency maps originates from loss estimation. Finally, the data shown in Figs. 4, 5 and 6 were developed for a selected reference

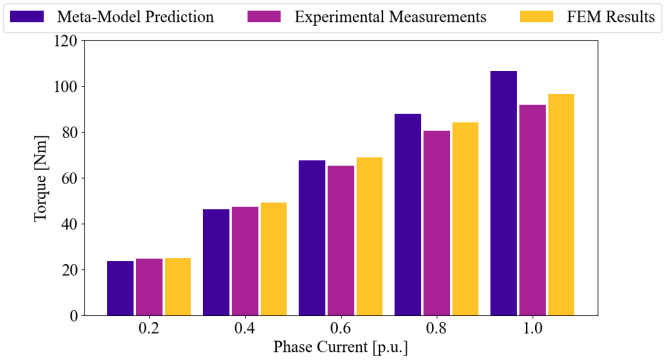

Fig. 10: Torque with $i_q = I_{ph}$ and $i_d = 0$A for different current levels.

design: k_{si} = 0.652, h_g = 1.784, k_{w_t} = 0.535, $k_{h_{pm}}$ = 0.776, $k_{w_{pm}}$ = 0.438, $k_{w_{br}}$ = 0.519, d_{br} = 2.42 and h_y = 11.4. This machine design has a maximum torque of 65.2Nm and was selected to show that the working points selected are sufficient to characterize any design in the domain.

2) GPR Geometry - New Geometry, Full Characterization: For the meta-model's second module, 512 different designs were simulated throughout the 14 working points selected during the first module. This data was then used to fit the Geometry $\mathcal{GP}$'s, described in detail in Fig 3 and on the context of the proposed meta-model architecture in Fig. 2. The prototype design was used for the evaluation of the second module. This design is new to the train data-set, not being included in the 512 different designs mentioned previously. The results show good agreement between the meta-model output and the results from 256 FEM simulations, with most of the efficiency map is under a 0.5%pt of discrepancy, as shown in Fig. 9. The ψ_d and ψ_q maps present a maximum of 2mWb of discrepancy, as illustrated in Fig. 7 and Fig. 8. This validates the capability of the proposed meta-modeling strategy to deal successfully with new and unknown designs.

B. Experimental Validation

The comparison between torque prediction using FEM simulation, experimental data [6] [12] and the meta-model output are compared in Fig. 10. It was used a FEM correction factor of 0.9 to detailed the very high magnetic saturation of this prototype. The meta-model output agrees with both the FEM simulations and experimental data. The low deviation is a consequence of the low errors in predicting ψ_q and ψ_d. However, the increasing error with the load suggests that the proposed meta-model should also adopt a strategy to deal with the heavy magnetic saturation.

VI. Conclusion

This study proposes a novel meta-modelling strategy that takes advantage of $\mathcal{GP}$'s regression capabilities and leverages the regression results through the use of governing physical equations to estimate the performance of a new design. The proposed meta-model also uses an adapted version of PSD that allows for a single point selection during adaptive sampling in a multi-output GPR problem.

The novel meta-model strategy showed good agreement with FEM results and experimental data, with a majority of the domain being predicted within a 5% error, making it suitable to be used in optimization problems to evaluate proposed designs, instead of recurring to FEM models. The generation of efficiency maps by the proposed meta-model allows its use in optimization problems considering drive cycles and multiple working points, for a fraction of the computational effort that a FEM only solution would require.

Acknowledgment

The support of the StandUp for Energy strategic government initiative, the Swedish Electromobility Center, Anna Maria Lundins Stipendiefond, and in the US of the National Science Foundation (NSF) Graduate Research Fellowship under Grant No. 2239063 is gratefully acknowledged. Any opinions, findings, and conclusions or recommendations expressed in this material are those of the authors and do not necessarily reflect the views of the sponsoring organizations.

References

[1] M. Cheng, X. Zhao, M. Dhimish, W. Qiu, and S. Niu, "A review of data-driven surrogate models for design optimization of electric motors," *IEEE Transactions on Transportation Electrification*, pp. 1 – 1, 2024.

[2] M. F. B. Omar, E. B. Sulaiman, I. A. Soomro, M. Z. B. Ahmad, and R. Aziz, "Design optimization methods for electrical machines: A review," *J. Electr. Eng. Technol.*, vol. 18, pp. 2783 – 2800, 2023.

[3] M. Rosu, P. Zhou, D. Lin, D. M. Ionel, M. Popescu, F. Blaabjerg, V. Rallabandi, and D. Staton, *Fem-Based Analysis Techniques for Electrical Machine Design*, 2018, pp. 45–108.

[4] M. Omar, M. Bakr, and A. Emadi, "Switched reluctance motor design optimization: A framework for effective machine learning algorithm selection and evaluation," *IEEE Transportation Electrification Conference and Expo (ITEC)*, 2024.

[5] E. V. Bonilla, K. M. A. Chai, and C. K. I. Williams, "Multi-task gaussian process prediction," *Proceedings of the 20th International Conference on Neural Information Processing Systems*, pp. 153 – 160, 2007.

[6] A. Fatemi, D. M. Ionel, M. Popescu, and N. A. O. Demerdash, "Design optimization of a high torque density spoke-type PM motor for a formula E race drive cycle," *IEEE Transactions on Industry Applications*, vol. 54, no. 5, pp. 4343–4354, 2018.

[7] B. Praslicka, N. Taran, and C. Ma, "An ultra-fast method for analyzing ipm motors at multiple operating points using surrogate models," *IEEE Transportation Electrification Conference and Expo (ITEC)*, pp. 868 – 873, 2022.

[8] B. Poudel and E. Amiri, "Deep learning based design methodology for electric machines: Data acquisition, training and optimization," *IEEE Access*, vol. 11, pp. 18 281 – 18 290, 2023.

[9] P. Asef and C. Vagg, "A physics-informed bayesian optimization method for rapid development of electrical machines," *Scientific Reports*, vol. 4526, no. 14, 2024.

[10] S. Stipetic, J. Goss, D. Zarko, and M. Popescu, "Calculation of efficiency maps using a scalable saturated model of synchronous permanent magnet machines," *IEEE Transactions on Industry Applications*, vol. 54, no. 5, pp. 4257 – 4267, 2018.

[11] C. Marchand, M. Djami, M. H. Hassan, G. Krebs, P. Dessante, and L. Belhaj, "Metamodel-based electric vehicle powertrain optimization: A drive cycle approach," *IEEE International Electric Machines and Drives Conference (IEMDC)*, pp. 1 – 5, 2023.

[12] A. Fatemi, *Design Optimization of Permanent Magnet Machines Over a Target Operating Cycle Using Computationally Efficient Techniques*. (2016). Dissertations (1934-). 662.

[13] C. E. Rasmussen and C. K. I. Williams, "Gaussian processes for machine learning," vol. 18, no. 8, pp. 912 – 923, 2006.